J Electroceram
DOI 10.1007/s10832-014-9967-4

Thermal stability of amorphous Zn-In-Sn-O films

Diana E. Proffit · Thomas Philippe · Jonathan D. Emery · Qing Ma · Bruce D. Buchholz · Peter W. Voorhees · Michael J. Bedzyk · Robert P. H. Chang · Thomas O. Mason

Received: 11 June 2014 / Accepted: 31 August 2014

Abstract Isochronal annealing of amorphous Zn and Sn codoped In_2O_3 (a-ZITO) films was performed at the Synchrotron so that to extract, in situ, important kinetic nucleation and growth parameters from a single constant-rate heating experiment. First, amorphous Zn and Sn codoped In_2O_3 films were deposited via pulsed laser deposition and subjected to post-deposition annealing treatments to study their stability against crystallization. Crystallization on glass and ĉ-sapphire occurred near the same temperature, however higher codoping levels resulted in increased crystallization temperatures. Post-deposition anneal crystallization temperatures were found to be higher than the substrate temperatures required to grow crystalline films during deposition. Then, a-ZITO films were subjected to a constant temperature ramp during in situ grazing-incidence X-ray diffraction experiments. Crystallization of films on both glass and ĉ-sapphire showed similar gradual crystallization behavior between 300 and 345 °C and strong (111) texturing, which suggests the influence of surface energy minimization during crystallization. The activation energy was found to be 2.87 eV using Johnson-Mehl-Avrami analysis. This work presents the advantages of in situ experiments to study nucleation and growth during crystallization of transparent conducting oxides.

Keywords Amorphous · Crystallization · Zn-In-Sn-O · Transparent conducting oxides

1 Introduction

Transparent conducting oxides (TCOs) combine high conductivity (>1000 S/cm) with high transparency (>80 % in ~100 nm thin films) in the visible spectrum. As a result, these materials are useful as electrodes in a wide variety of electronic applications such as flat-panel displays, photovoltaics, and light-emitting diodes [1–3]. Interest in flexible electronics and the resulting need for low processing temperatures to enable deposition on plastics has driven research on amorphous (a-) TCOs. These materials provide lower surface roughness, improved interfacial contacts, and better mechanical properties as compared to crystalline TCOs [4–9].

The industry standard for high conductivity TCOs has historically been Sn-doped In_2O_3 (ITO), but the volatile cost of indium has encouraged a search for low-In alternatives [10, 11]. A promising ITO-alternative is the solid solution $In_{2-2x}Sn_xZn_xO_3$ ($x \leq 0.4$) (ZITO) in which In_2O_3 is codoped with equal amounts of Sn and Zn [12, 13]. The high level of codoping significantly reduces the indium content, yet the material retains the bixbyite structure common to In_2O_3 and ITO. Amorphous ZITO has electrical and optical properties similar to those of its crystalline counterparts [10, 14].

The thermal stability and crystallization temperature of a-ZITO films are important considerations in the processing and application of these materials, yet relatively little work has been done to date in this area. In fact, to our knowledge, no effort to date has been made to understand the ZITO

D. E. Proffit · T. Philippe (✉) · J. D. Emery · B. D. Buchholz · P. W. Voorhees · M. J. Bedzyk · R. P. H. Chang · T. O. Mason
Department of Materials Science and Engineering, Northwestern University, Evanston, IL 60208, USA
e-mail: thomas.philippe1984@gmail.com

T. Philippe
Groupe de Physique des Matériaux (GPM), Normandie Université, UMR CNRS 6634 BP 12, Avenue de l'Université, 76801 Saint Etienne du Rouvray, France

Q. Ma
DND-CAT, Northwestern Synchrotron Research Center at Advanced Photon Source, Argonne, IL 60439, USA

M. J. Bedzyk
Department of Physics and Astronomy, Northwestern University, Evanston, IL 60208, USA

Published online: 11 September 2014

crystallization process. The primary focus of this manuscript is to isochronally monitor the crystallization process of $In_{1.4}Sn_{0.3}Zn_{0.3}O_3$ (ZITO30) via grazing-incidence wide-angle X-ray scattering (GIWAXS) during a temperature ramp. The in situ procedure will allow for the extraction of kinetic parameters related to nucleation and growth during crystallization with a single constant-rate heating experiment. In addition, we will compare the post-deposition annealing temperature needed to induce crystallization within 1 h at two codoping levels. The results will be discussed within the context of previous work, including the effect of deposition temperature on film crystallinity and properties.

2 Background

An understanding of the effect of post-deposition annealing temperature on structure is critical to processing considerations for TCOs. Currently, the studies on post-deposition annealing have dealt only with the influence on properties without much consideration for the annealing crystallization temperature [15, 16]. Because electrical properties may change before the onset of crystallization, as is seen in In_2O_3 [17] and ITO [17, 18], using these properties as a metric for structural changes can be misleading.

Annealing studies are helpful, but a fundamental understanding of the crystallization process is more widely applicable. Although the crystallization process in ZITO has not been studied, studies of crystallization processes in In_2O_3 and ITO have been completed using several methods. Real-time in situ X-ray diffraction (XRD) during constant heating showed crystallization occurs between 165 and 210 °C for In_2O_3 and 185 and 230 °C for ITO [19, 20]. The crystallization of both In_2O_3 and ITO was then modeled using a chemical reaction rate equation, yielding activation energies of 2.31±0.06 eV and 2.41 eV, respectively, with a reaction order of 0.75 [19, 20].

In addition, GIWAXS patterns of ITO taken during isothermal crystallization were used to estimate the crystalline phase fraction (which is proportional to the integrated diffraction peak intensity) during the transformation, which was then compared to the Johnson-Mehl-Avrami equation [21]. The results found activation energies of 1.3±0.2 eV [22] and 0.77 eV [23, 24] with a reaction order between 2 and 4. It is important to note that these activation energies are lower than those found using the chemical reaction rate equation.

Lastly, the crystallization process in ITO was also studied using a time-resolved optical reflectivity study, but it was noted that the reflectivity, like the electrical properties, changes before the onset of crystallization and therefore interpretation can be complex [25]. Crystallization in ITO appears to be preceded by an ordering and/or relaxation process with a similar activation energy to crystallization, but that obeys first order reaction kinetics [22].

Finally, a discussion of thermal stability would be incomplete without mentioning previous work examining the effect of substrate temperature during deposition. It has generally been observed that the addition of Zn or an increase in Zn concentration raises the necessary substrate temperature to induce crystallization during film deposition [8, 14, 15, 26, 27]. This result is reasonable when comparing the annealing crystallization temperature of In_2O_3 (<250 °C) to those of IZO (>600 °C) [6] and ZTO (>500 °C) [28, 29]. Also, doping In_2O_3 with Sn has been shown to slightly increase crystallization temperature compared to undoped In_2O_3 [17, 20]. X-ray absorption spectroscopy studies of the local structures in a-ZITO indicate a difference in both bond distance and coordination around Zn between the crystalline and amorphous films, which could explain the increase in crystallization activation energy [30, 31].

The substrate temperature during ZITO film deposition plays an important role not just in determining structure, but also in determining electrical and optical properties, which are of direct interest for potential applications. A few studies regarding this parameter have been performed on pulsed laser deposited ZITO30 films [14], RF magnetron cosputtered ITO-ZnO films with compositions of ~65 at.% In and ~11 at.% Sn (the balance being Zn) [8], and other RF magnetron cosputtered ITO-ZnO films with varying Zn at.% [15, 16]. The onset of crystallization results in a drop in the electronic mobility, which is likely due to electron scattering at interfaces such as amorphous/crystalline phase boundaries and grain boundaries. Carrier concentrations do not change significantly with changes in substrate temperature. Overall, conductivity increases until just before crystallization, and then decreases as the degree of thin film crystallinity increases [8, 14]. Similar trends in electrical properties are also shown by Liu et al. [15], but are not directly correlated with structural measurements. The increase of conductivity up to the onset of crystallization, which has been observed during post-annealing of In_2O_3 [17] and ITO [22], suggests the influence of defect concentration homogenization and/or relaxation of internal local strains [14]. Film density in amorphous films is also known to increase with deposition and/or annealing temperature [32], which may also play a role. Bandgap and optical transmittance are generally constant as the substrate temperature varies over the range in which the amorphous-to-crystalline phase transition is observed [8, 14, 15].

3 Experimental procedure

Two a-ZITO30 ($In_{1.4}Sn_{0.3}Zn_{0.3}O_3$) films and two a-ZITO70 ($In_{0.6}Sn_{0.7}Zn_{0.7}O_3$) films were grown by pulsed laser deposition (PLD) at an ambient of 7.5 mTorr O_2 without substrate heating. One film of each Zn concentration was grown on glass and ĉ-sapphire substrates 10×10 mm^2. The film thicknesses were estimated to be ~250 nm based on calibrated

deposition rates. The PLD system employs a 248 nm KrF excimer-laser operated at 2 Hz with a 25-ns pulse duration and pulse energy of 200 mJ/pulse. The beam was focused to a 1 × 2 mm^2 spot and rastered across the rotating (5 rpm) target to prevent local heating. The target-substrate separation was fixed at 10 cm. A dense, hot-pressed, ceramic target of $In_{1.4}Sn_{0.27}Zn_{0.33}O_3$ composition used to deposit the ZITO30 film, and a ceramic target of nominal $In_{0.6}Sn_{0.7}Zn_{0.7}O_3$ composition was used to deposit the ZITO70 film.

The pre- and post-anneal film crystallinity was investigated by GIXRD using a Rigaku ATX-G Thin Film Diffraction Workstation (Tokyo, Japan) with 8.04 keV X-rays and a flux of ~10^8 photons/s. The incident angle was fixed at θ=0.5° during the 2θ scan from ~10 to 80° with a step size of either 0.05° or 0.5° and a scan rate of 2°/min. After baseline GIXRD measurements, the films were subjected to post-deposition annealing in air at 200 °C and re-measured. The annealing process included a 5 °C/min ramp up from room temperature to the hold temperature, a 1 h hold, and a 5 °C/min ramp down to room temperature (the cooling rate slowed to the natural cooling rate of the box furnace at low temperatures). If the post-anneal GIXRD data exhibited no crystalline peaks, a subsequent anneal (and re-measurement) was performed at a hold temperature 50 °C higher than the preceding measurement up to a maximum hold temperature of 600 °C. Above this temperature, substrate softening could affect amorphous phase stability.

Two additional a-ZITO30 thin films were deposited via PLD on ~10×20 mm^2 ĉ-sapphire and glass substrates without substrate heating. An ambient atmosphere of 5 mTorr O_2 was used for these films. Film thickness was estimated to be ~500 nm based upon calibrated deposition rates.

These films were enclosed in an evacuated (1×10^{-3} Torr) beryllium dome X-ray scattering environmental cell and mounted on a pyrolytic boron nitride-coated pyrolytic graphite (PBN/PG) heating stage for in situ wide-angle X-ray scattering (GIWAXS) measurements. The cell was mounted on a four-circle diffractometer at the Dupont-Northwestern-Dow Collaborative Access Team (DND-CAT) 5BM-D beamline at the Advanced Photon Source (Argonne National Laboratory, Argonne, IL). X-rays were monochromated to 19.5 keV using a Si(111) crystal and were subsequently focused to a ~100 μm (vertical) by ~0.5 mm (horizontal) beam by a Sagittal bending mirror. The X-ray penetration depth was predominantly limited to the film volume by tuning the incident grazing angle to 0.6°, and thereby significantly enhancing the film-to-substrate signal ratio. Scattered X-rays were collected with a 165 mm diameter MarCCD area detector positioned ~315 mm from the sample. Sample-to-detector distance and detector tilt were calibrated using a lanthanum hexaboride standard.

In-house GIXRD measurements indicated that the films do not crystallize below 200 °C. Therefore, during in situ measurements the thin films were heated to 200 °C at a rate of 6 °C/min, at which point they were subjected to a 10 min hold before acquiring scattering data. During scattering measurements, the films were heated to 450 °C at a rate of 0.5 °C/min, then subjected to a 10 min hold, and subsequently ramped down to 20 °C at a rate of 6 °C/min or (at low temperatures) the natural cooling rate of the system. Images were continuously acquired using a detector exposure time of 19 s (plus 5 s readout) until diffraction from crystalline domains was observed near 346 °C. At this point exposure time was decreased to 10 s (plus 5 s readout) to avoid detector saturation. During the measurement the incident beam alignment was adjusted periodically to correct for the effects of thermal expansion of the components of the cell, which lead to a small drift in the incident angle over time.

4 Results and discussion

Figure 1 shows a selection of GIXRD patterns taken after consecutive post-deposition annealing treatments in air for the ZITO30 (top panel) and ZITO70 (bottom panel) films deposited on glass. The films deposited on ĉ-sapphire exhibited the same behavior as those on glass. It was somewhat unexpected that the films crystallized at the same temperature on glass as on ĉ-sapphire, because ZITO can form an epitaxial film with ĉ-sapphire (which we expected to lower the activation energy for crystallization). In the epitaxial films, the (222) ZITO planes are parallel to the (0001) Al_2O_3 planes and the $\{5\bar{5}0\}$ ZITO planes match to the $\{3\bar{3}00\}$ Al_2O_3 planes with only a 2.8 % mismatch [33].

The ZITO30 film remained amorphous after the annealing treatment at 300 °C but was at least partially crystallized after the annealing treatment at 350 °C, and therefore the hold temperature that induces crystallization in ZITO30 under these annealing conditions is between these two temperatures. In contrast, the ZITO70 film did not crystallize at even the highest annealing temperature (600 °C) in this study. These annealing crystallization temperature onsets are higher than those found for both In_2O_3 and ITO [19, 20]. These results indicate that an increase in codoping level increases amorphous phase stability, which is consistent with experiments determining the deposition substrate temperature needed to induce crystallization [14, 27].

Additionally, by comparing the substrate temperature that induces crystallization during deposition to the post-anneal temperature necessary to crystallize the film (150–200 °C [27] and 300–350 °C, respectively, for ZITO30), it is clear that substrate temperature needed for crystallization during growth is consistently lower. The relatively large differences between the local structures around Zn in amorphous and crystalline ZITO in conjunction with the increased amount of Zn likely play a role in increasing the activation energy of crystallization with increasing codoping level [30, 31].

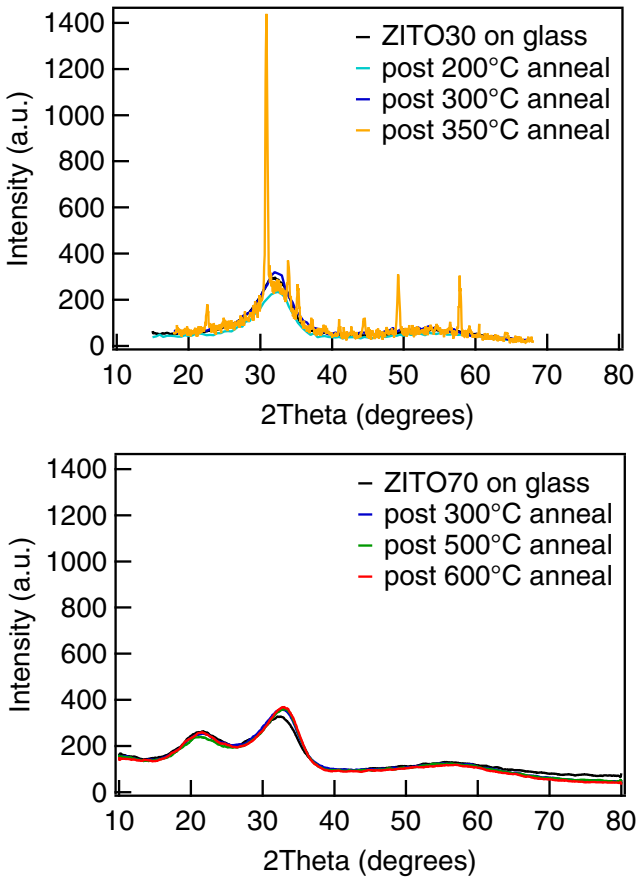

Fig. 1 GIXRD patterns taken after sequential post-deposition annealing treatments (in air) on the ZITO30 (*top panel*) and ZITO70 (*bottom panel*) films deposited on glass

Figure 2 shows representative GIWAXS patterns from the ZITO30 film deposited on ĉ-sapphire measured at 240, 330, and 410 °C. These three patterns represent the "before", "during", and "after" stages of crystallization. The data are displayed as a function of in-plane $q_{xy}=4\pi\sin(2\theta_{xy}/2)/\lambda$ and out-of-plane $q_z=2\pi\sin(\alpha_f/2)/\lambda$ momentum transfer, where $2\theta_{xy}$ and α_f are the in-plane and out-of-plane scattering angles, and λ is the X-ray wavelength. The Debye-Scherrer rings corresponding to the (211), (222), and (400) lattice planes are indicated in Fig. 2b–c, and the broad amorphous ring is marked in Fig. 3a. The patterns taken at 330 and 410 °C show the emergence of significant (111) texturing as evidenced by the anisotropic intensity modulations about the Debye-Sherrer rings at constant $q_{Tot}=(q_{xy}^2+q_z^2)^{1/2}$. It should be noted that this texturing is also present in the crystallized film grown on glass (not shown), indicating that additional factors other than substrate orientation, such as surface energy, influence film texturing. The GIWAXS patterns show that crystallization of ZITO30 occurs between 300 and 345 °C. Although the width of the temperature range of crystallization (45 °C) is the same as that for In_2O_3 and ITO, these results show that a-ZITO crystallizes at a higher temperature [19, 20], indicating a more stable amorphous phase.

Due to the similarity between the ZITO30 films on ĉ-sapphire and glass, only measurements completed on the film on ĉ-sapphire are presented herein. The data were first converted to reciprocal space coordinates using the Nika software package [34] in the Igor Pro environment. In order to avoid the complicated near-specular (~70-110°) and near in-plane (0-15°, 165-180°) signal regions, radial q_{Tot} -scans were extracted by integrating intensity within a limited azimuthal slice of 150±15°. The near-specular region is distorted in reciprocal space due to the experimental geometry, and the in-plane region displays shadowing from the sample holder. Additionally, this integration accommodates the strong (111) out-of-plane preferential orientation of the crystallized films by including contributions from both preferentially and randomly oriented crystallites. We note that the ratio of the peak intensities for the selected region closely resembles patterns from untextured bixbyite films.

The resulting q_{Tot} linescans clearly displayed peaks from the (200), (211), (222), (400), (411) lattice planes as well as from the amorphous phase. The peaks were fit with Gaussian line shapes in order to extract integrated intensities, peak positions, and peak widths. The integrated peak intensities were normalized to the maximum observed intensity for the respective phase (crystalline/amorphous), which is proportional to the volume fraction of that phase.

The integrated peak intensities as a function of temperature from the (211) ring and the amorphous ring of the film on ĉ-sapphire are shown in Fig. 3. Because the strongest peaks, the (222) and (400), have significant overlap with the broad amorphous ring, analysis was limited to the third-strongest (211) ring. The statistical uncertainty associated with the amorphous peak volume fraction is low, but the uncertainty of the crystalline volume fraction is relatively high due to the relatively low counting statistics for the (211) peak. A small difference (~3-5°) between the crystallization temperatures extracted from each of the two curves is significantly less than the discrepancy (~20°) resulting from differing definitions of the crystallization temperature (appearance of crystalline diffraction signal versus 50 % crystallized) and the small difference is likely due to the background signal dominating a weak crystalline diffraction signal at low temperature.

The normalized amorphous intensity as a function of temperature was subjected to kinetic parameter fitting. The fitting method was developed based upon the Johnson-Mehl-Avrami equation [21]. The crystallized volume fraction is defined as $X(t)=1-\exp(-Kt^n)$, where t is time, n is the reaction order, and $K=K_0 exp(-Q/k_BT)$. K_0 is a pre-factor, Q is the activation energy, k_B is the Boltzmann constant, and T is the temperature. Because the heating rate is constant, temperature at time t can be defined as $T=T_0+At$, where T_0 is temperature at $t=0$, and A is the heating rate. It is convenient to use the fraction of amorphous phase, Y (where $Y=1-X$) such that,

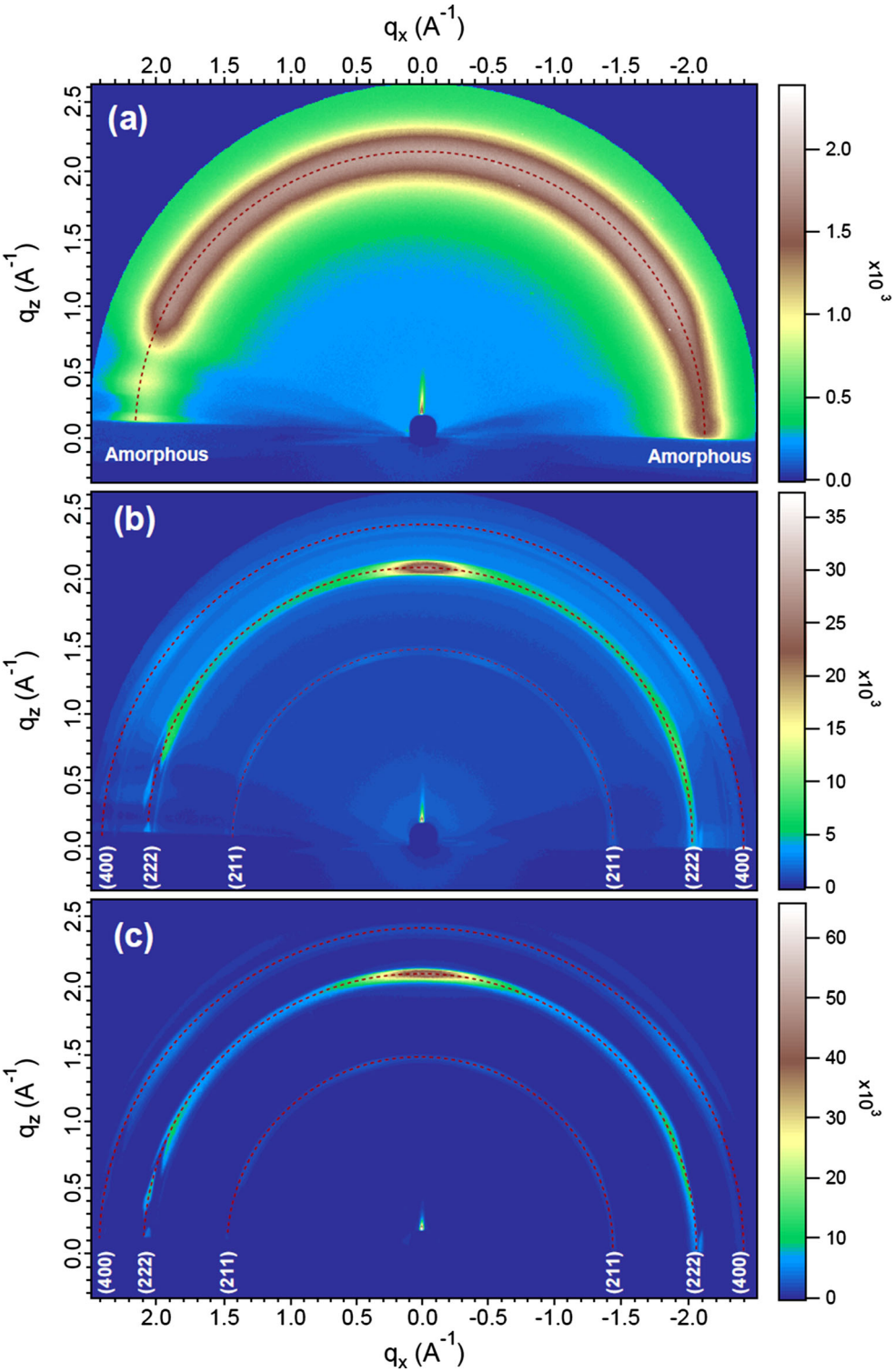

Fig. 2 In situ GIWAXS patterns taken at (**a**) 240, (**b**) 330, and (**c**) 410 °C during crystallization of a ZITO30 film deposited ĉ-sapphire. The patterns exhibit only amorphous scattering at low temperature (a), then diffraction signals from crystalline phases appear (b), and finally the sample has been completely crystallized and no amorphous scattering is observed (c). The anisotropic intensity pattern about the Debye-Scherrer ring indicate strong (111) texturing of the crystallized ZITO film

$$\ln Y = -K_0 \exp(-Q/RT)\left(\frac{T-T_0}{A}\right)^n \quad (1)$$

Analysis requires three fitting parameters: K_0, Q, and n. Known parameters included A (0.5 °C/min) and T_0. Because the experimental parameters stabilized at 280 °C and no crystalline signal was yet observable, this temperature was chosen as most appropriate for T_0. The choice of T_0 generally can affect the value of the exponent (n), but has a much smaller effect on the calculated value of the activation energy.

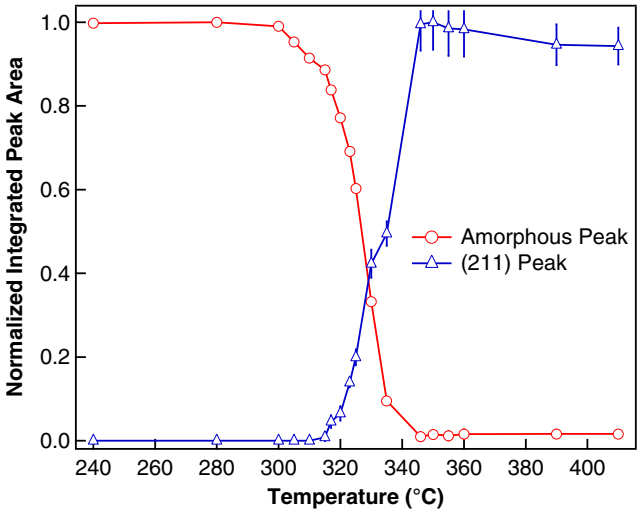

Fig. 3 Integrated peak area versus temperature for the amorphous (*red circles*) and (211) peaks (*blue triangles*) from ZITO30 GIWAXS patterns

The most reasonable fit for the normalized amorphous intensity (i,e, amorphous phase fraction), shown in Fig. 4, gives an activation energy (Q) of 2.87 eV, a reaction order (n) of 2.87, and a pre-factor (K_0) of 1.5×10^{13}. Increasing or decreasing T_0 by 10 °C did not significantly change the activation energy or reaction order.

The activation energy for ZITO30 is higher than that calculated for In_2O_3 (2.31±0.06 eV) and ITO (2.41 eV) in similar experiments using a different calculation method [19, 20]. This result agrees well with the higher crystallization temperature measured in ZITO. Also, the ZITO activation energy is quite high compared to other values for In_2O_3 and ITO reported in the literature (0.67±0.18 eV [25], 0.77 eV [23], and 1.3±0.2 eV). The results are consistent with the post-deposition annealing study discussed above.

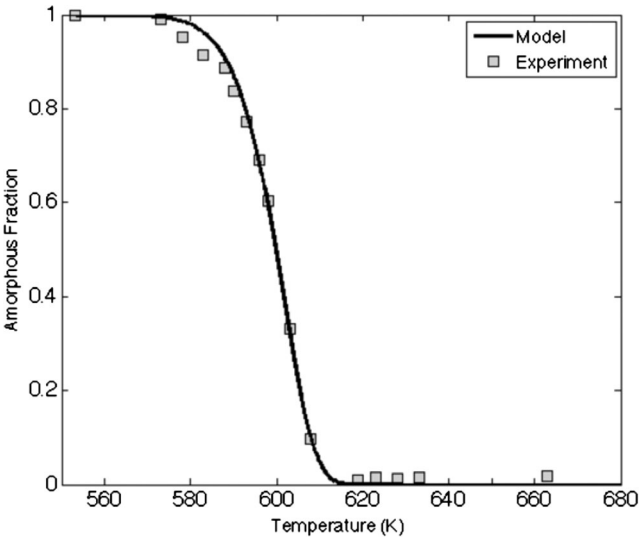

Fig. 4 Fraction of the amorphous phase versus temperature calculated from GIWAXS of ZITO30, along with the calculated best fit based upon the Johnson-Mehl-Avrami equation

There are two processes that result in a reaction order of 3. The crystallization process could occur via site-saturated nucleation with three-dimensional growth. However, this clearly cannot be the case when the crystallizing region contacts the substrate or surface of the film. Thus deviations from this prediction would be expected when the crystalline volume fraction is large. For a constant nucleation rate, a value of 3 is also possible with two-dimensional growth in the film. The strong (111) texture of the films is consistent with a heterogeneous nucleation process along the substrate or surface of the film, and thus is consistent with this case. Further isothermal crystallization experiments are required to clarify the amorphous-to-crystalline transition mechanism.

5 Conclusions

Post-deposition annealing of ZITO30 and ZITO70 films showed that crystallization occurs at lower annealing temperatures for ZITO30 than ZITO70 films. However, crystallization occurs within the same temperature range for films of similar composition deposited on glass and ĉ-sapphire substrates. The higher codoping level in ZITO70 increases the amorphous phase stability due to the increase in the amount of Zn, consistent with studies on the effect of codoping level on the substrate temperature needed to induce crystallinity during deposition. Previous work showed that the differences in the local structures around Zn between a-ZITO films and crystalline ZITO films are larger than those around In or Sn [30, 31]. The effect of post-deposition annealing on film electrical and optical properties will be explored in future work.

The in situ GIWAXS measurements during constant rate heating of ZITO30 films demonstrated that crystallization of ZITO30 occurs gradually from 300 to 345 °C for films deposited on both glass and ĉ-sapphire. This temperature range is higher than that measured for In_2O_3 and ITO, and is attributed to the higher activation energy for crystallization in ZITO than in In_2O_3 and ITO. ZITO30 crystallizes with strong (111) texturing when deposited on both ĉ-sapphire and glass, which is consistent with heterogeneous nucleation of crystals along the surfaces of the film. The in situ procedure allowed to extract important kinetic parameters related to crystallization with a single constant-rate heating experiment.

Overall, ZITO is a promising alternative to In_2O_3 and ITO for applications requiring better amorphous phase stability. The adjustment of codoping levels in ZITO was shown to strongly influence the crystallization temperature, which may be useful when applying these materials to various processing and application needs.

Acknowledgments This work was supported by the MRSEC program of the National Science Foundation (DMR-1121262). A portion of the work done by DBB and RPHC was also supported by the U.S. Department of Energy, Office of Science, Office of Basic Energy Sciences under Award Number DE-FG02-06ER46320. Portions of this work were performed at the DuPont-Northwestern-Dow Collaborative Access Team (DND-CAT) located at Sector 5 of the Advanced Photon Source (APS). DND-CAT is supported by E.I. DuPont de Nemours & Co., The Dow Chemical Company and Northwestern University. Use of the APS, an Office of Science User Facility operated for the U.S. Department of Energy (DOE) Office of Science by Argonne National Laboratory, was supported by the U.S. DOE under Contract No. DE-AC02-06CH11357. This work made use of the J.B.Cohen X-Ray Diffraction Facility supported by the MRSEC program of the National Science Foundation (DMR-1121262) at the Materials Research Center of Northwestern University. DEP acknowledges support of an NSF Graduate Research Fellowship.

References

1. E. Fortunato, D. Ginley, H. Hosono, and D. C. Paine, "Transparent conducting oxides for photovoltaics," MRS Bull., 32 [3] 242–247 (2007).
2. J.F. Wager, D.A. Keszler, R.E. Presley, *Transparent electronics* (Springer, New York, 2008)
3. D.S. Ginley, H. Hosono, D.C. Paine, *Handbook of transparent conductors* (Springer, New York, 2010)
4. T. Kamiya, H. Hosono, Material characteristics and applications of transparent amorphous oxide semiconductors. NPG Asia Mater. **2**, 15–22 (2010)
5. J. Liu, D.B. Buchholz, R.P.H. Chang, A. Facchetti, T.J. Marks, High-performance flexible transparent thin-film transistors using a hybrid gate dielectric and amorphous zinc indium tin oxide channel. Adv. Mater. **22**(21), 2333–2337 (2010)
6. M.P. Taylor, D.W. Readey, M.F.A.M. Van-Hest, C.W. Teplin, J.L. Alleman, M.S. Dabney, L.M. Gedvilas, B.M. Keyes, B. To, J.D. Perkins, D.S. Ginley, The remarkable thermal stability of amorphous In-Zn-O transparent conductors. Adv. Funct. Mater. **18**(20), 3169–3178 (2008)
7. J.A. Jeong, H.K. Kim, S.I. Na, Low resistance and high transparent amorphous IZTO electrode cosputtered by linear facing target sputtering for organic photovoltaics. Electrochem. Solid-State Lett. **12**(9), J80–J82 (2009)
8. G.S. Heo, Y. Matsumoto, I.G. Gim, J.W. Park, K.Y. Kim, T.W. Kim, Fabrication of cosputtered Zn-In-Sn-O films and their applications to organic light-emitting diodes. Solid State Comm **149**(41–42), 1731–1734 (2009)
9. G.S. Heo, Y. Matsumoto, I.G. Gim, H.K. Lee, J.W. Park, T.W. Kim, Transparent conducting amorphous Zn-In-Sn-O anode for flexible organic light-emitting diodes. Solid State Comm **150**(3–4), 223–225 (2010)
10. C.A. Hoel, T.O. Mason, J.F. Gaillard, K.R. Poeppelmeier, Transparent conducting oxides in the ZnO-In2O3-SnO2 System. Chem. Mater. **22**(12), 3569–3679 (2010)
11. D.S. Ginley, C. Bright, Transparent conducting oxides. MRS Bull. **25**(8), 15–18 (2000)
12. G.B. Palmer, K.R. Poeppelmeier, T.O. Mason, Conductivity and transparency of ZnO/SnO2-cosubstituted In2O3. Chem. Mater. **9**(12), 3121–3126 (1997)
13. S.P. Harvey, T.O. Mason, D.B. Buchholz, R.P.H. Chang, C. Körber, A. Klein, Carrier generation and inherent Off-stoichiometry in Zn,Sn Co-doped indium oxide (ZITO) bulk and thin film specimens. J. Am. Ceram. Soc. **91**(2), 467–472 (2008)
14. D.B. Buchholz, J. Liu, T.J. Marks, M. Zhang, R.P.H. Chang, Control and characterization of the structural, electrical, and optical properties of amorphous zinc-indium-tin oxide thin films. ACS Appl. Mater. Interf **1**(10), 2147–2153 (2009)
15. D.S. Liu, C.S. Sheu, C.T. Lee, C.H. Lin, Thermal stability of indium tin oxide thin films co-sputtered with zinc oxide. Thin Solid Films **516**(10), 3196–3203 (2008)
16. K.J. Chen, F.Y. Hung, S.J. Chang, S.P. Chang, Y.C. Mai, Z.S. Hu, A study on crystallization, optical and electrical properties of the advanced ZITO thin films using co-sputtering system. J. Alloys Compd. **509**(8), 3667–3671 (2011)
17. A. Rogozin, M. Vinnichenko, N. Shevchenko, U. Kreissig, A. Kolitsch, W. Moller, Real-time evolution of electrical properties and structure of indium oxide and indium tin oxide during crystallization. Scr. Mater. **60**(4), 199–202 (2009)
18. A. Rogozin, N. Shevchenko, M. Vinnichenko, F. Prokert, V. Cantelli, A. Kolitsch, W. Moller, Real-time evolution of the indium tin oxide film properties and structure during annealing in vacuum. Appl. Phys. Lett. **85**(2), 212–214 (2004)
19. F.O. Adurodija, L. Semple, R. Brüning, Real-time in situ crystallization and electrical properties of pulsed laser deposited indium oxide thin films. Thin Solid Films **492**, 153–157 (2005)
20. F.O. Adurodija, L. Semple, R. Brüning, Crystallization process and electro-optical properties of In2O3 and ITO thin films. J. Mater. Sci. **41**(21), 7096–7102 (2006)
21. M. Avrami, Kinetics of phase change. II transformation-time relations for random distribution of nuclei. J. Chem. Phys. **8**, 212–224 (1940)
22. D.C. Paine, T. Whitson, D. Janiac, R. Berseford, C.O. Wang, B. Lewis, A study of Low temperature crystallization of amorphous thin film indium Tin oxide. J. Appl. Phys. **85**, 8445–8450 (1999)
23. H. Wulff, M. Quaas, H. Steffen, R. Hippler, In situ studies of diffusion and crystal growth in plasma deposited thin ITO films. Thin Solid Films **377**, 418–424 (2000)
24. M. Quaas, H. Steffen, R. Hippler, H. Wulff, Investigation of diffusion and crystallization processes in thin ITO films by temperature and time resolved grazing incidence X-ray diffractometry. Surf. Sci. **540**(2–3), 337–342 (2003)
25. C.W. Ow-Yang, D. Spinner, Y. Shigesato, D.C. Paine, A time-resolved reflectivity study of the amorphous-to-crystalline transformation kinetics in dc-magnetron sputtered indium tin oxide. J. Appl. Phys. **83**(1), 145–154 (1998)
26. G.S. Heo, I.G. Gim, J.W. Park, K.Y. Kim, T.W. Kim, Effects of substrate temperature on properties of ITO-ZnO composition spread films fabricated by combinatorial RF magnetron sputtering. J. Solid State Chem. **182**(10), 2937–2940 (2009)
27. D.B. Buchholz, D.E. Proffit, M.D. Wisser, T.O. Mason, R.P.H. Chang, Electrical and band-gap properties of amorphous zinc–indium–tin oxide thin films. Prog. Nat. Sci: Mater Int **22**(1), 1–6 (2012)
28. E. Cetinorgu, S. Goldsmith, Z. Barkay, R.L. Boxman, The dependence of filtered vacuum arc deposited ZnO-SnO2 thin films characteristics on substrate temperature. J. Phys. D. Appl. Phys. **39**(24), 5245–5251 (2006)
29. E. Cetinorgu, S. Goldsmith, R.L. Boxman, The effect of post-deposition annealing on the optical properties of filtered vacuum arc deposited ZnO-SnO2. J. Phys. Condens. Matter **19**(25), 256206 (2007)
30. D.E. Proffit, D.B. Buchholz, R.P.H. Chang, M.J. Bedzyk, T.O. Mason, Q. Ma, X-ray absorption spectroscopy study of the local structures of crystalline Zn-In-Sn oxide thin films. J. Appl. Phys. **106**(11), 113524–113526 (2009)
31. D.E. Proffit, Q. Ma, D.B. Buchholz, R.P.H. Chang, M.J. Bedzyk, T.O. Mason, Structural and physical property studies of

amorphous Zn-in-Sn-O thin films. J. Am. Ceram. Soc. **95**(11), 3657–3664 (2012)
32. D. Bruce Buchholz, Z. Li, M.J. Bedzyk, R.P.H. Chang, Differences between amorphous indium oxide thin films. Prog in Nat Sci: Mater Int (2013). doi:10.1016/jpnsc.2013.08.004
33. M. Zhang, D.B. Buchholz, S.J. Xie, R.P.H. Chang, Twinned domains in epitaxial ZnO/SnO2-cosubstituted In2O3 thin films. J. Cryst. Growth **308**, 376–381 (2007)
34. J. Ilavsky, Nika – software for 2D data reduction. J. Appl. Cryst. **45**, 324–328 (2012)